



## Ultraviolet-C persistent luminescence from Lu<sub>2</sub>SiO<sub>5</sub>:Pr<sup>3+</sup> persistent phosphor for solar-blind optical tagging

Journal:	<i>Dalton Transactions</i>
Manuscript ID	DT-ART-03-2021-000791.R1
Article Type:	Paper
Date Submitted by the Author:	13-Apr-2021
Complete List of Authors:	<p>Yan, Shao; Shandong University, Key Laboratory for Liquid-Solid Structure Evolution and Processing of Materials, Ministry of Education  Liang, Yanjie; Shandong University, Key Laboratory for Liquid-Solid Structure Evolution and Processing of Materials, Ministry of Education  Chen, Yafei; King Fahd University of Petroleum &amp; Minerals, Center for Integrative Petroleum Research  Liu, Jingwei; Shandong University, Key Laboratory for Liquid-Solid Structure Evolution and Processing of Materials, Ministry of Education  Chen, Dongxun; Shandong University, Key Laboratory for Liquid-Solid Structure Evolution and Processing of Materials, Ministry of Education  Pan, Zhengwei; King Fahd University of Petroleum &amp; Minerals, Center for Integrative Petroleum Research</p>

**Ultraviolet-C persistent luminescence from  $\text{Lu}_2\text{SiO}_5\text{:Pr}^{3+}$  persistent phosphor for solar-blind optical tagging**

Shao Yan,<sup>a</sup> Yanjie Liang,<sup>\*a,c</sup> Yafei Chen,<sup>b</sup> Jingwei Liu,<sup>a</sup> Dongxun Chen,<sup>a</sup> and Zhengwei Pan<sup>\*b</sup>

*<sup>a</sup>Key Laboratory for Liquid-Solid Structure Evolution and Processing of Materials, Ministry of Education, Shandong University, Jinan 250061, P. R. China. E-mail: yanjie.liang@sdu.edu.cn*

*<sup>b</sup>Center for Integrative Petroleum Research, College of Petroleum Engineering and Geosciences, King Fahd University of Petroleum and Minerals, Dhahran 31261, Kingdom of Saudi Arabia. E-mail: zhengwei.pan@gmail.com*

*<sup>c</sup>Advanced Medical Research Institute, Shandong University, Jinan 250012, P. R. China.*

## Abstract

Visible and infrared persistent phosphors have gained considerable attention in recent years and are being widely used as glow-in-the-dark materials in dark environments. In contrast, the progress on persistent phosphors emitting at the other end of the spectrum, i.e., the shorter-wavelength ultraviolet-C (UVC; 200-280 nm), is rather slow. Here we report the design and synthesis of a well-performing Pr<sup>3+</sup>-doped UVC emissive persistent phosphor, Lu<sub>2</sub>SiO<sub>5</sub>:Pr<sup>3+</sup>, which exhibits intense UVC persistent luminescence peaking at 270 nm and long persistence time of more than 12 h after excitation by a 254 nm UV lamp. Besides, the UVC persistent luminescence of a UV pre-irradiated sample can be repeatedly revived after repeated short-illumination by low-energy white light via a process called photostimulated persistent luminescence. Owing to the distinct spectral features of UVC light and the self-sustained luminescence property, the UVC persistent luminescence of Lu<sub>2</sub>SiO<sub>5</sub>:Pr<sup>3+</sup> persistent phosphor can be clearly monitored and imaged by a corona camera in bright environments including direct sunlight and indoor light. The Lu<sub>2</sub>SiO<sub>5</sub>:Pr<sup>3+</sup> persistent phosphor is expected to find promising application in the covert optical tagging field.

## 1. Introduction

Ultraviolet C (UVC) light with a wavelength shorter than 280 nm has found various important applications in the fields of water sterilization, photochemistry, confidential communication, and solar-blind detection due to its distinct wavelength features.<sup>1-6</sup> For instance, in terms of disinfection, shorter-wavelength UVC radiation can destroy the DNA/RNA in living microorganisms so that they cannot reproduce, thus making them harmless. Buonanno and coworkers have recently utilized long-time UVC illumination to kill the COVID-19 effectively.<sup>7</sup> For solar-blind detection, the absence of UVC light on the Earth surface results in zero background interference from sunlight or artificial lighting sources, enabling the luminescence signal to be monitored and recorded all time and all weather with high-accuracy positioning by a UVC corona camera.<sup>8</sup> Currently, the most frequently used UVC light source on the market is dominated by the low-pressure mercury vapour discharge lamp with an emission wavelength at 254 nm. However, for some special applications such as solar-blind imaging and microbial inactivation, it is highly desirable that there are solid-state light sources that can emit strong and long persistent UVC radiation for an appreciable time from minutes to many hours without the need of external power sources, a special luminescence phenomenon commonly referred to as persistent luminescence.<sup>9-11</sup>

The past two decades have witnessed the significant progress of persistent luminescence materials research, involving the discovery of new persistent phosphors, the development of new characterization methods and the in-depth understanding of persistent luminescence mechanism.<sup>12-17</sup> As a result of extensive research, there are an array of well-known persistent luminescence materials emitting in the visible and infrared spectral regions.<sup>18-25</sup>

More importantly, the strong and long persistent visible and infrared emissions make these phosphors quickly found exciting applications in night-vision surveillance, medical diagnostics, optical information storage, and so on.<sup>26-29</sup> In contrast, however, persistent phosphors emitting at the other end of the spectrum - the shorter-wavelength UVC spectral region - are relatively lacking, even though there are growing demands in the UVC persistent phosphors for advanced applications ranging from sterilization to solar-blind imaging.

For UVC photoluminescence, trivalent praseodymium,  $\text{Pr}^{3+}$ , is a promising UVC emitter, which can generate emissions from UVC to infrared, owing to the interactions between the non-4f states and the abundant 4f energy levels.<sup>30,31</sup> J. T. W. de Hair has reported the broad UV emission originated from  $4f^15d^1 \rightarrow 4f^2$  transition of  $\text{Pr}^{3+}$  in  $\text{BaY}_4\text{Si}_5\text{O}_{17}:\text{Pr}^{3+}$  phosphor in an earlier study.<sup>32</sup> Since then, a series of  $\text{Pr}^{3+}$  doped UVC phosphors have been developed, with the representative ones including  $\text{YBO}_3:\text{Pr}^{3+}$ ,  $\text{YPO}_4:\text{Pr}^{3+}$ ,  $\text{LuPO}_4:\text{Pr}^{3+}$ , etc.<sup>33-35</sup> Nevertheless, compared with the significant achievements in  $\text{Pr}^{3+}$  activated UVC photoluminescence materials, the research progress on  $\text{Pr}^{3+}$  doped UVC persistent luminescence materials is rather slow. Yang et al. reported persistent UVC luminescence in  $\text{Pr}^{3+}$ -doped  $\text{Cs}_2\text{NaYF}_6$  phosphor with a persistence time of  $\sim 2$  h after the excitation of high-energy X-ray.<sup>36</sup> However, long-time radioactive X-ray excitation is essential to achieve UVC persistent luminescence, while the most common UV lamps cannot be used as excitation sources. Wang and coworkers recently synthesized  $\text{Pr}^{3+}$ -doped silicate-based UVC persistent phosphors using a solid-state reaction method, which can be effectively charged by a standard 254 nm lamp and exhibit UVC persistent luminescence peaking at 265–270 nm.<sup>37</sup> Among them,  $\text{Pr}^{3+}$ -doped oxyorthosilicate UVC persistent phosphors only

exhibit an afterglow duration of  $\sim 3$  h. The development of these silicate-based UVC persistent phosphors is a clear breakthrough in persistent luminescence research and applications. In virtue of the peculiar UVC emission exhibited by  $\text{Pr}^{3+}$  together with the appealing energy trap properties in silicate-based inorganic hosts, the development and in-depth study of more reliable  $\text{Pr}^{3+}$ -doped UVC persistent phosphors with excellent performance are highly desirable, which will greatly expand the UVC persistent luminescence materials library and enable some new applications where the UVC emission is needed.

Here, we report the synthesis of  $\text{Pr}^{3+}$ -doped  $\text{Lu}_2\text{SiO}_5$  persistent phosphors via the sol-gel method followed by heat treatment. In comparison to the  $\text{Lu}_2\text{SiO}_5:\text{Pr}^{3+}$  phosphors synthesized by the high-temperature solid-state reaction method, the samples obtained by the sol-gel technique exhibit much better persistent luminescence performance, which can emit persistent UVC light peaking at around 270 nm for more than 12 h after the excitation of a 254 nm UV lamp. The  $\text{Lu}_2\text{SiO}_5:\text{Pr}^{3+}$  persistent phosphor also exhibits a photo-stimulated persistent luminescence capability. Remarkably, the solar-blind optical tagging application is demonstrated in bright indoor and outdoor environments by taking advantage of the zero UVC background on the Earth surface. Besides the detailed spectral studies, comprehensive investigations on the trap charging and detrapping processes in the material were also conducted by using the thermoluminescence technique to better understand the underlying UVC persistent luminescence mechanism.

## 2. Materials and methods

### 2.1 Materials

$\text{Lu}_2\text{O}_3$  (99.99%),  $\text{Pr}(\text{NO}_3)_3 \cdot 6\text{H}_2\text{O}$  (99.99%),  $\text{NaNO}_3$  (99.99%), and citric acid

monohydrate ( $C_6H_8O_7 \cdot H_2O$ , 99.5%) were purchased from Aladdin Reagents. Nitric acid ( $HNO_3$ , 68 wt%), ethanol and tetraethyl orthosilicate (TEOS, 98%) were obtained from Sinopharm Chemical Reagents.  $Lu(NO_3)_3$  solution of 0.5 mol/L was prepared by dissolving  $Lu_2O_3$  in nitric acid at elevated temperature. All of the above chemical reagents were directly used for sample preparation without further purification.

## 2.2 Synthesis of $Lu_2SiO_5:Pr^{3+}$ phosphors

A series of  $Lu_{2-x}SiO_5:xPr^{3+}$  ( $0 \leq x \leq 0.03$ ) phosphors were prepared by a sol-gel method followed by heat treatment. In a typical procedure, to prepare  $Lu_{1.995}SiO_5:0.5\%Pr^{3+}$  phosphor, the solutions were mixed with 40 mL ethanol, 50  $\mu$ L  $Pr(NO_3)_3$  solution (0.25 mol/L), 400  $\mu$ L  $NaNO_3$  solution (0.25 mol/L) and 9.975 mL  $Lu(NO_3)_3$  solution (0.5 mol/L). Next, citric acid (0.01 mol) was added to the above mixed solution. After the citric acid was completely dissolved, 0.557 mL of TEOS was added to the solution with constant stirring in 60 °C water bath for ~3 hours until a transparent sol was formed. The obtained sol was dried at 100 °C for 24 hours and then ground to obtain the precursor powder. The resulting precursor powder was sintered at 900 °C for 2 h in air to remove the organic matter. Then the pre-sintered material was again ground to a fine powder and pressed into discs with diameters of ~11 mm using a 30-ton dry pressing machine. The discs were sintered at 1250 °C in air for 6 h to form the  $Lu_2SiO_5:Pr^{3+}$  solid ceramic discs.

## 2.3 Characterization

Crystal structure and phase composition were measured by powder X-ray diffraction (XRD, DMAX-2500PC, Rigaku) with a scanning speed of  $10^\circ \text{ min}^{-1}$ . The crystal structure refinement was carried out using the General Structure Analysis System (GSAS) program. Diffuse reflectance spectra were recorded by ultraviolet-visible spectroscopy (UV-Vis,

Specord). The photoluminescence spectra and persistent luminescence spectra at room temperature were studied by an FLS1000 spectrofluorometer (Edinburgh Instrument) equipped with a 450 W Xenon lamp, a photomultiplier tube (measurement range, 200-900 nm) and an InGaAs detector (measurement range, 800-1600 nm). Thermoluminescence (TL) spectra were recorded using a SL18 thermoluminescence setup (Guangzhou Rongfan Science and Technology Co., Ltd; heating rate, 4 °C/s). Before all the spectral measurements, the samples were heat-treated in a furnace at 450 °C to completely empty the energy traps in the material. The indoor and outdoor UVC imaging was recorded by an Ofil DayCor Luminar HD corona camera. The camera can take bi-spectral UVC (240-280 nm)-visible images. The visible image shows the samples and the background, while the UVC image shows the UVC radiation as an area of red color. The final image taken by the corona camera is an overlay image after the superimposition of a UVC image onto a visible image. The persistent luminescence emission power intensities were obtained with a Newport 1936-R optical power meter and a Newport 918D-UV-OD3R UV enhanced silicon photodetector. The power intensity was measured following the procedures described in the reference.<sup>37</sup>

### **3. Results and Discussion**

#### **3.1 Crystallinity and structure analysis of Lu<sub>2</sub>SiO<sub>5</sub>:Pr<sup>3+</sup> phosphor**

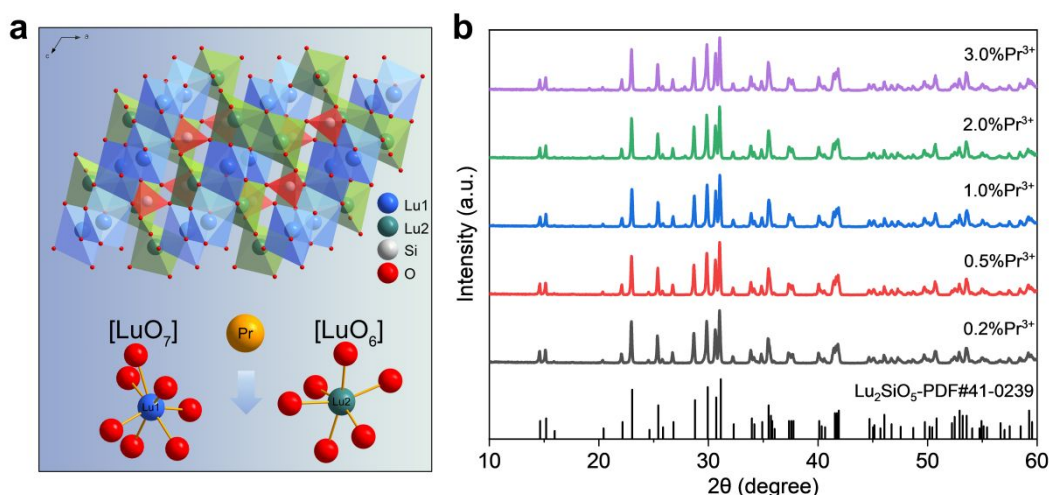


**Fig. 1** Crystal structure and XRD analysis of  $\text{Lu}_2\text{SiO}_5:\text{Pr}^{3+}$  phosphor. (a) A schematic diagram of the crystal structure of  $\text{Lu}_2\text{SiO}_5$ . (b) XRD patterns of  $\text{Lu}_{2-x}\text{SiO}_5:x\%\text{Pr}^{3+}$  phosphors ( $x = 0.2, 0.5, 1, 2, 3$ ).

The  $\text{Lu}_2\text{SiO}_5$  crystal belongs to the  $C2/c$  space group with a monoclinic structure, which has the cell parameters of  $a = 14.254 \text{ \AA}$ ,  $b = 6.641 \text{ \AA}$ ,  $c = 10.241 \text{ \AA}$ , and  $\beta = 122.2^\circ$ .<sup>38</sup> The simulated crystal structure of  $\text{Lu}_2\text{SiO}_5$  is shown in Fig. 1a. In the  $\text{Lu}_2\text{SiO}_5$  lattice, two kinds of crystallographic orientations of Lu ions with the coordination numbers of 6 and 7 are observed, which are labelled as Lu1 and Lu2, respectively. Lu1 can coordinate with five oxygen atoms of  $[\text{SiO}_4]$  and two isolated oxygen atoms to form the polyhedron (blue balls in Fig. 1a). Correspondingly, Lu2 can coordinate with four oxygen atoms of  $[\text{SiO}_4]$  and two isolated oxygen atoms to form the polyhedron (green balls in Fig. 1a). The phase composition and crystallinity of the as-prepared  $\text{Lu}_2\text{SiO}_5:\text{Pr}^{3+}$  phosphors were first investigated by XRD. Figure 1b shows the XRD patterns of  $\text{Lu}_2\text{SiO}_5:\text{Pr}^{3+}$  phosphors doped with different amounts of  $\text{Pr}^{3+}$  ( $0.2 \leq x \leq 3$ ). All diffraction peaks can be well indexed to the monoclinic  $\text{Lu}_2\text{SiO}_5$  phase (JCPDS 41-0239). No detectable XRD peaks corresponding to the secondary phase were observed, indicating that the pure  $\text{Lu}_2\text{SiO}_5$  phase can be prepared

under the present synthesis conditions. With the increase of  $\text{Pr}^{3+}$  doping concentration, there is no apparent change of the crystal structure of  $\text{Lu}_2\text{SiO}_5$  host due to the similar valence state and ionic radius between  $\text{Lu}^{3+}$  and  $\text{Pr}^{3+}$ .

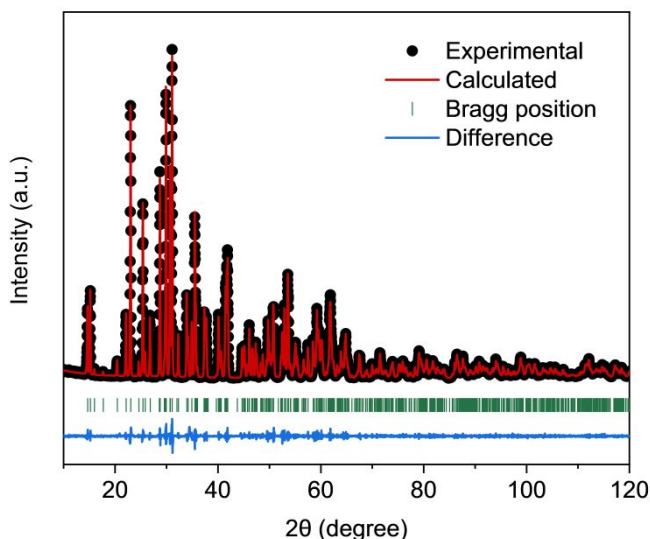


**Fig. 2** The Rietveld refinement of  $\text{Lu}_2\text{SiO}_5:0.5\%\text{Pr}^{3+}$  phosphor.

The calculated and experimental results as well as the differences in the Rietveld refinement of  $\text{Lu}_2\text{SiO}_5:0.5\%\text{Pr}^{3+}$  phosphor are shown in Fig. 2. The monoclinic  $\text{Lu}_2\text{SiO}_5$  crystal system was used as the initial model for refinement. In view of the closeness of the ionic radius and equivalent charge between  $\text{Pr}^{3+}$  and  $\text{Lu}^{3+}$ , the substitution of  $\text{Pr}^{3+}$  for  $\text{Lu}^{3+}$  in the host lattice is reasonable from a crystallochemical point of view. The detected and calculated XRD patterns match well with each other and the reliability parameters of the refinement are  $R_{wp} = 7.45\%$ ,  $R_p = 5.26\%$ , and  $\chi^2 = 1.639$ , which manifests that the as-synthesized phosphor is pure  $\text{Lu}_2\text{SiO}_5$  phase. The refined lattice parameters with  $a = 14.254 \text{ \AA}$ ,  $b = 6.643 \text{ \AA}$ ,  $c = 10.256 \text{ \AA}$  further indicate that the crystal structure of  $\text{Lu}_2\text{SiO}_5$  remains almost unchanged after the introduction of  $\text{Pr}^{3+}$  ions. Detailed crystallographic data is shown in Table S1 in the Supporting Information.

### 3.2 Photoluminescence properties of $\text{Lu}_2\text{SiO}_5:\text{Pr}^{3+}$ phosphor

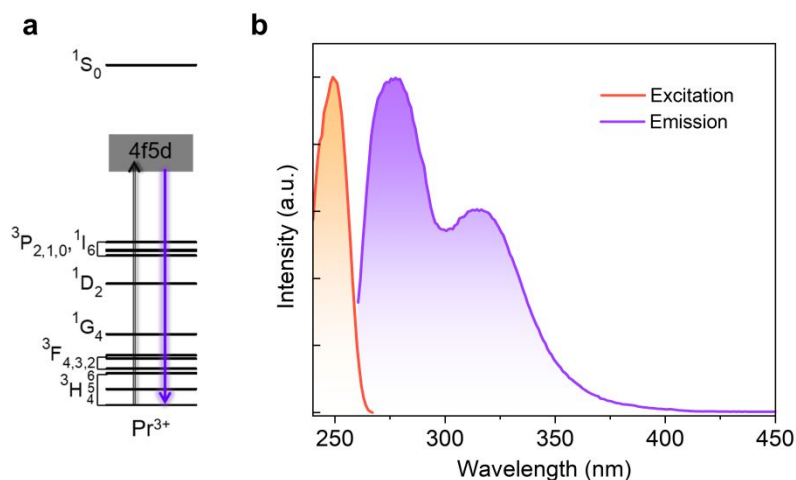


**Fig. 3** Energy level scheme of the  $\text{Pr}^{3+}$  ion and photoluminescence spectra of the  $\text{Lu}_2\text{SiO}_5:\text{Pr}^{3+}$  phosphor. (a) Energy level scheme of  $\text{Pr}^{3+}$   $4f^2 \rightarrow 4f^15d^1$  configuration and the possible optical transition. (b) Excitation and emission spectra of  $\text{Lu}_2\text{SiO}_5:\text{Pr}^{3+}$  phosphor at room temperature. The emission spectrum is obtained under 248 nm light excitation, and the excitation spectrum is acquired by monitoring the 280 nm emission.

The occurrence of  $\text{Pr}^{3+}$   $4f^15d^1 \rightarrow 4f^2$  transitions in a solid need to satisfy two general conditions: the energy of the  $\text{Pr}^{3+}$   $4f^15d^1$  configuration is below the  $^1S_0$  level and there is a very small Stokes shift of  $4f^15d^1 \rightarrow 4f^2$  emission (less than  $3000 \text{ cm}^{-1}$ ),<sup>31</sup> as shown in Fig. 3a. The photoluminescence emission and excitation spectra of  $\text{Lu}_2\text{SiO}_5:\text{Pr}^{3+}$  phosphor are shown in Fig. 3b. When exciting with 248 nm UV light, the emission spectra are composed of two broad emission bands distributed in the UV spectral region from  $\sim 260 \text{ nm}$  to  $\sim 380 \text{ nm}$ , with the maxima at 280 nm and 313 nm, respectively. These UV emission bands have been reported in earlier studies of  $\text{Lu}_2\text{SiO}_5:\text{Pr}^{3+}$  scintillator crystal and films,<sup>39,40</sup> which can be attributed to the  $4f^15d^1 \rightarrow 4f^2$  interconfigurational transitions of the  $\text{Pr}^{3+}$  emitter. Photoluminescence emission spectra of  $\text{Lu}_2\text{SiO}_5:\text{Pr}^{3+}$  phosphors with different  $\text{Pr}^{3+}$  doping concentration is shown in Supplementary Fig. S1. The photoluminescence emission spectra of  $\text{Lu}_2\text{SiO}_5:\text{Pr}^{3+}$  phosphor at different temperatures were also investigated. As shown in

Supplementary Fig. S2, the emission spectra at different temperatures exhibit similar profiles including the shape and peak position with increasing the temperature. However, the decrease of emission intensity is significantly evident and the relative emission intensity at 175 °C is only 1.7% of that at 25 °C. Therefore, the UVC emission is greatly suppressed at high temperature due to the thermal ionization quenching.<sup>41</sup> The excitation spectrum monitored at 280 nm emission exhibits a broad absorption band ranging from 230 nm to 260 nm with the peak at 248 nm, which can be assigned to the  $4f^2 \rightarrow 4f^1 5d^1$  transition of  $\text{Pr}^{3+}$ . The broad excitation band in the UVC region demonstrates that the  $\text{Lu}_2\text{SiO}_5:\text{Pr}^{3+}$  phosphor can be effectively excited by a standard 254 nm mercury lamp.

### 3.3 Persistent luminescence properties of $\text{Lu}_2\text{SiO}_5:\text{Pr}^{3+}$ phosphor

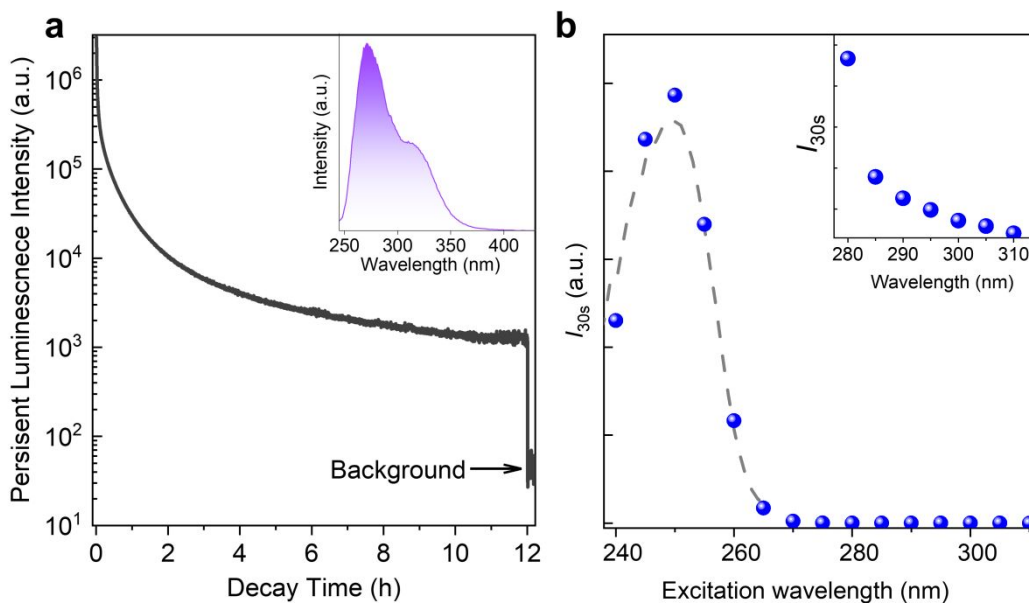


**Fig. 4** Persistent luminescence properties of  $\text{Lu}_2\text{SiO}_5:\text{Pr}^{3+}$  phosphor. (a) UVC persistent luminescence decay curve monitored at 270 nm after irradiation by 254 nm UV lamp for 15 min. The upper inset shows the persistent luminescence emission spectrum acquired at 10 min decay after the stoppage of the irradiation. (b) Persistent luminescence excitation spectrum obtained by plotting the persistent luminescence intensity ( $I_{30s}$ ) monitored at 270

nm as a function of the excitation wavelengths over the 240-310 nm spectral range. The sample was pre-irradiated for 5 min at each measured wavelength using a xenon arc lamp. For comparison, the dash-line curve shows the photoluminescence excitation spectrum.

When the 254 nm UV light excitation was ceased, the  $\text{Lu}_2\text{SiO}_5:\text{Pr}^{3+}$  phosphor exhibits long-lasting persistent luminescence in the UV spectral region. Figure 4a presents long-lasting persistent luminescence decay curve of  $\text{Lu}_2\text{SiO}_5:0.5\%\text{Pr}^{3+}$  phosphor monitored at 270 nm at room temperature after irradiation with a 254 nm UV lamp for 15 min. The data were recorded as a function of the afterglow intensity at 270 nm *versus* decay time and the recording lasted for 12 h. The persistent UVC emission intensity drops quickly in the initial stage (0-2 h) and then decays slowly (2-12 h). After 12 h of decay, the UVC persistent luminescence at 270 nm can still be measured. The UVC persistent luminescence power intensity of the  $\text{Lu}_2\text{SiO}_5:\text{Pr}^{3+}$  phosphor in the first several minutes was recorded used a Newport 1936-R optical power and energy meter and a Newport 918D-UV-OD3R UV enhanced silicon photodetector, as shown in Supplementary Table S2 and Supplementary Fig. S3. The initial UVC persistent luminescence power intensities at 1 s, 15 s, and 30 s were calculated as 11.35 mW/m<sup>2</sup>, 6.98 mW/m<sup>2</sup>, and 1.62 mW/m<sup>2</sup>, respectively. The persistent luminescence decay curves with different  $\text{Pr}^{3+}$  doping concentrations were also measured and the results are given in Supplementary Fig. S4. The persistent luminescence emission spectrum (upper insert in Fig. 4a) exhibits a similar profile with that of the photoluminescence emission spectrum, indicating that the persistent UVC emission at 270 nm originates from the  $4f^15d^1 \rightarrow 4f^2$  transition of  $\text{Pr}^{3+}$ . Furthermore, the reciprocal persistent luminescence intensity ( $I^{-1}$ ) as a function of decay time ( $t$ ) was also plotted in  $I^{-1}$  versus  $t$  coordinates, as shown in Supplementary Fig. S5. The  $I^{-1} \sim t$  at 2–12 h decay period can be

well fitted by a straight line, indicating that the tunnelling-related process is probably responsible for the long-lasting UVC persistent luminescence in the  $\text{Lu}_2\text{SiO}_5:\text{Pr}^{3+}$  phosphor.<sup>42,43</sup> Compared with the  $\text{Lu}_2\text{SiO}_5:\text{Pr}^{3+}$  phosphors synthesized by the sol-gel method here, the samples obtained by high-temperature solid-state reaction method show poor persistent luminescence performance, including weaker persistent luminescence intensity, shorter duration time ( $\sim 3$  h), and stronger visible persistent emission, as shown in Supplementary Fig. S6.

In order to study the effectiveness of different excitation wavelengths on the UVC persistent luminescence of  $\text{Lu}_2\text{SiO}_5:\text{Pr}^{3+}$  phosphor, monochromic light between 240 to 310 nm in 5 nm steps was used to excite the sample for 5 min and the persistent luminescence decay curves monitored at 270 nm were recorded after the irradiation, as shown in Supplementary Fig. S7. The persistent luminescence excitation spectrum was obtained by recording the persistent luminescence intensity at a decay time of 30 s ( $I_{30\text{s}}$ ) with the variation of excitation wavelengths, as the blue balls shown in Fig. 4b. It can be markedly noticed that the UVC afterglow can only be achieved by high-energy UV light excitation with a wavelength shorter than 310 nm. Meanwhile, the UVC persistent luminescence intensity steadily increases as the excitation wavelength decreases, reaching the maximum at 250 nm. Furthermore, the profile of persistent luminescence excitation spectrum of  $\text{Lu}_2\text{SiO}_5:\text{Pr}^{3+}$  (Fig. 4b) is almost identical to that of the photoluminescence excitation spectrum (Fig. 3b), indicating that the excitation of  $\text{Pr}^{3+}$  leads to UVC persistent luminescence.

### 3.4 Photochromic properties of $\text{Lu}_2\text{SiO}_5:\text{Pr}^{3+}$ phosphor

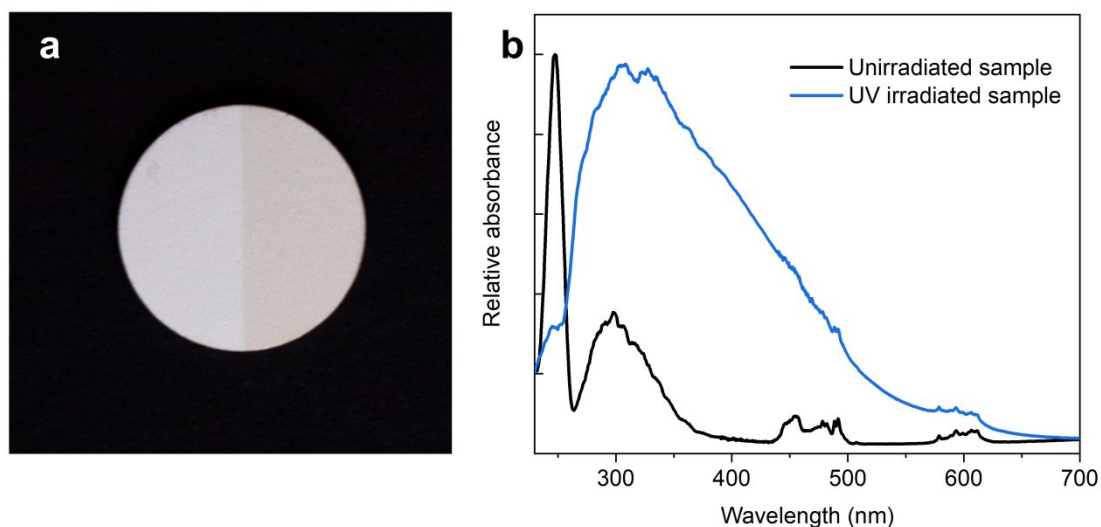


**Fig. 5** UV-irradiation-induced coloration of  $\text{Lu}_2\text{SiO}_5:\text{Pr}^{3+}$  phosphor. (a) Digital pictures of a  $\text{Lu}_2\text{SiO}_5:\text{Pr}^{3+}$  phosphor disc. The right side of the disc was pre-irradiated with a 254 nm UV lamp for 10 min, while the left side was covered by black paper. (b) Absorption spectra of  $\text{Lu}_2\text{SiO}_5:\text{Pr}^{3+}$  disc with and without UV irradiation.

When irradiating a  $\text{Lu}_2\text{SiO}_5:\text{Pr}^{3+}$  phosphor disc with a 254 nm UV lamp in the indoor-lighting environment, it is found that the body color of  $\text{Lu}_2\text{SiO}_5:\text{Pr}^{3+}$  disc changes from white to pale reddish-brown (Fig. 5a), a unique phenomenon called photochromism.<sup>44</sup> The UV light-induced coloration can maintain at room temperature for several days. But it can be quickly bleached by heating the disc at around 400 °C. The diffuse reflectance spectra of the phosphor with and without UV excitation are measured to further study the photochromism caused by UV irradiation, as shown in Fig. 5b. For the sample without UV irradiation, the strong absorption bands between 230-350 nm, 430-500 nm and 580-620 nm are ascribed to the  $4f \rightarrow 4f5d$ ,  $^3\text{H}_4 \rightarrow ^3\text{P}_{0,1,2}$  and  $^3\text{H}_4 \rightarrow ^1\text{D}_2$  transitions of  $\text{Pr}^{3+}$  ion, respectively. Compared with the unirradiated sample, additional intense absorption bands in the UV and visible spectral regions are observed in the UV-irradiated sample, resulting in the pale reddish-brown color change of  $\text{Lu}_2\text{SiO}_5:\text{Pr}^{3+}$  phosphor disc. In view of the

coloration phenomenon in other well-performing persistent phosphors reported before,<sup>44</sup> it is concluded that the UV irradiation induced coloration can be derived from the formation of photochromic centers, which can serve as electron traps to store excitation energy and play a critical part in the long-lasting persistent luminescence decay process.

### 3.5 Thermoluminescence properties of $\text{Lu}_2\text{SiO}_5:\text{Pr}^{3+}$ phosphor

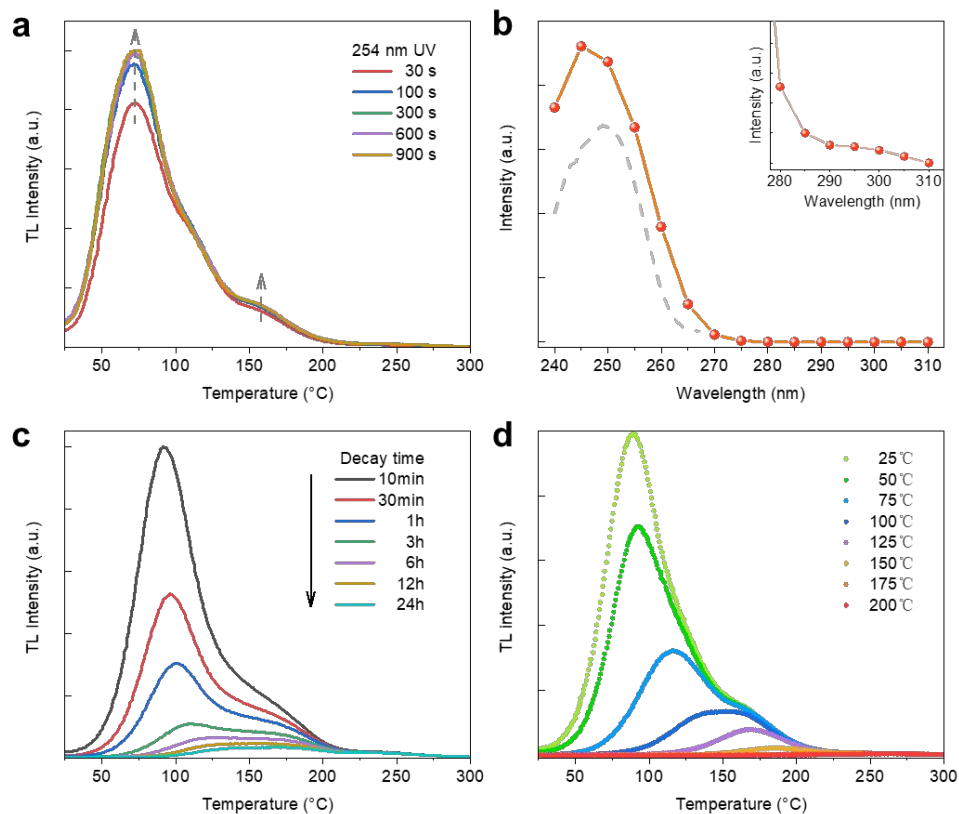


**Fig. 6** Thermoluminescence (TL) properties of  $\text{Lu}_2\text{SiO}_5:\text{Pr}^{3+}$  phosphor. (a) TL curves with excitation duration from 30 s to 15 min. TL curves were acquired at 60 s decay by monitoring at 270 nm over 25-300  $^{\circ}\text{C}$ . (b) TL excitation spectrum (orange ball curve) and photoluminescence excitation spectrum (grey dash curve) of  $\text{Lu}_2\text{SiO}_5:\text{Pr}^{3+}$  at room temperature. (c) TL curves for samples undergoing different decay times from 10 min to 24 h. The samples were pre-irradiated by a 254 nm UV lamp for 15 min. (d) TL curves for samples undergoing thermal cleaning experiment at different temperatures.

Thermoluminescence (TL) is the most effective and appropriate method to investigate the properties of energy traps and the energy transfer process between the traps and emitters in persistent phosphors.<sup>45,46</sup> Figure 6 presents the comprehensive investigations of trap charging and detrapping processes in  $\text{Lu}_2\text{SiO}_5:\text{Pr}^{3+}$  phosphor. Firstly, in order to investigate the influence of the excitation duration on the TL glow curves, the samples were irradiated by 254 nm UV light for different time ranging from 30 s to 900 s. As displayed in Fig. 6a, a direct relationship between the TL intensity and the excitation duration is clearly observed. Over 10 min excitation, the material appears to be fully charged. In this study, different lanthanide co-dopants ( $\text{Yb}^{3+}$ ,  $\text{Er}^{3+}$ ,  $\text{Tm}^{3+}$ ,  $\text{Eu}^{3+}$ , and  $\text{Ho}^{3+}$ ) were also introduced into  $\text{Lu}_2\text{SiO}_5:\text{Pr}^{3+}$  phosphors in order to enhance the TL intensity. However, it is found that the addition of lanthanide ions cannot significantly enhance the UVC persistent luminescence intensity and the TL intensity, as shown in Supplementary Fig. S8. Figure 6b shows the TL excitation spectrum (TLE), which is recorded as a function of TL intensity after each excitation *versus* the excitation wavelengths over 240-310 nm spectral range. The TL curves after excitation with different wavelengths between 240 and 310 nm in 5 nm steps are shown in Supplementary Fig. S9. As shown in Fig. 6b, the energy traps can be effectively charged under UVC light excitation (<280 nm). And the effectiveness increases greatly as the excitation moves to shorter wavelengths, reaching a maximum at 245 nm. Moreover, it is found that the TLE spectrum also shares an almost identical profile with the photoluminescence excitation spectrum (Fig. 3b), indicating that electrons that have been excited into the 4f5d state can be thermally liberated to the conduction band to fill the energy traps.<sup>47</sup> The long-lasting persistent luminescence is the exhaustive process of the trapped electrons in energy traps. Therefore, the TL curves at different decay times

from 10 min to 24 h after UV irradiation were recorded to reveal the release of trapped electrons involved in the persistent luminescence decay process. For the case of 60 s short decay, The TL curve displays a continuous broadband emission in the temperature range of 25 to 300 °C, as shown in Supplementary Fig. S10. Four emission peaks corresponding to traps with different depths were obtained by fitting the TL curve with Gaussian function, and the maxima of temperature were at 85.7 °C, 135.7 °C, 198.1 °C and 268.5 °C, respectively. The trap depths were estimated by Urbach method:<sup>12</sup>

$$E_t = \frac{T_m}{500}$$

Where  $E_t$  is the trap depth, and  $T_m$  is the Kelven temperature of the TL peaks. The calculated results were 0.72 eV, 0.82 eV, 0.94 eV and 1.08 eV, respectively. As the time-dependent TL curves shown in Fig. 6c, the intensity of emission bands at low temperature that corresponds to the shallow traps drops quickly, resulting in the band maximum of TL curves moving to the higher temperature. Meanwhile, the intensity of high-temperature band (deep traps) gradually decreases with the increase of decay time and the peak position almost keeps unchanged. The time-dependent TL results clearly indicate that the shallow traps are rapidly depleted in the first few hours, following by the empty of deep traps, which is consistent with the persistent luminescence decay curves in Fig. 4a. After 24 h long decay, a majority of the low-temperature TL band disappears and the intensity of high-temperature TL band (deep traps) looks very weak. However, it should be kept in mind that the TL measurements here cannot completely evaluate the storage capability of deep traps in  $\text{Lu}_2\text{SiO}_5:\text{Pr}^{3+}$  phosphor owing to the luminescence thermal quenching of 4f5d emitting state,<sup>48,49</sup> as confirmed in Supplementary Fig. S2. To further study the trap distribution in this material, thermal detrapping experiment was carried out at different

temperatures. The sample was pre-irradiated by a 254 nm UV lamp for 10 min at room temperature, then heated to the detrapping temperature to empty the traps below this temperature. After that, the sample was quickly cooled down to room temperature, and then the TL curve was recorded from 25 °C to 300 °C at 5 min decay. As shown in Fig. 6d, the peak maximum of TL curve gradually shifts to higher temperature with the increase of thermal detrapping temperature, accompanied by the sharp decrease of TL intensity. This result strongly demonstrates that there are continuous and wide distribution of traps in  $\text{Lu}_2\text{SiO}_5:\text{Pr}^{3+}$  phosphor.

### 3.6 Photostimulated UVC persistent luminescence (PSPL) in $\text{Lu}_2\text{SiO}_5:\text{Pr}^{3+}$ phosphor

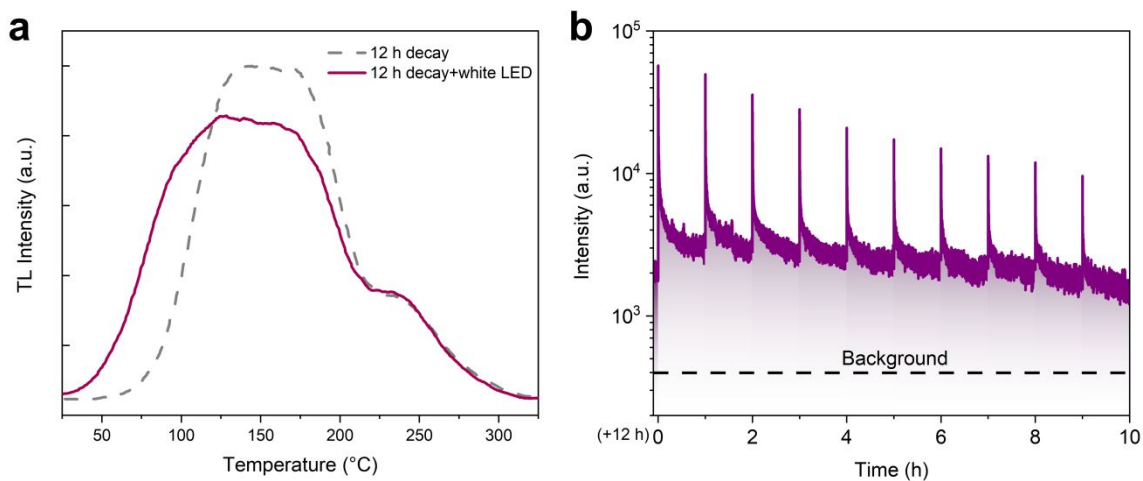


**Fig. 7** PSPL in  $\text{Lu}_2\text{SiO}_5:\text{Pr}^{3+}$  phosphor. (a) TL curves of 12 h-decayed samples with (solid-line curve) and without (dash-line curve) white LED illumination. (b) Repeated PSPL decay curves obtained on a 12 h-decayed phosphor disc. The monitoring emission wavelength is 270 nm. The 12 h-decayed sample was illuminated by a 550 Lumen white LED light for 10 s at every 1h for a total of 10 times.

The long-lasting self-sustained UVC luminescence of  $\text{Lu}_2\text{SiO}_5:\text{Pr}^{3+}$  phosphors open new opportunities for covert optical tagging in bright environments. However, the photostimulated luminescence (PSL) due to the stimulation of ambient light (sunlight or

indoor light) must be taken into consideration, and its contribution can be dominant when the ambient light is strong.<sup>37</sup> To study the influences of ambient light on the release of trapped energy, we illuminated 12 h-decayed  $\text{Lu}_2\text{SiO}_5:\text{Pr}^{3+}$  samples using a 550 Lumen white LED for 10 s, and recorded TL curves before and after low-energy white LED light illumination. As shown in Fig. 7a, the profile of TL curve is changed obviously after white LED illumination; that is, part of low temperature band (shallow traps) reappears and the intensity of high temperature band (deep traps) decreases, which is caused by the redistribution of the stored electrons in the traps.<sup>44</sup> Although the low-energy white light cannot directly charge the samples to achieve UVC persistent luminescence, it can trigger the liberation of the trapped electrons in deep traps, leading to the refilling of the depleted shallow traps for enhanced UVC persistent luminescence, a common spectral phenomenon in persistent phosphors termed photostimulated persistent luminescence (PSPL). Since only part of trapped electrons are photo-liberated after short-time white light illumination and a large amount of trapped electrons still remain in deep traps, the photostimulation of white light can be repeated many times (e.g., 10 times) over a long period (e.g., 10 h) until all deep traps are depleted, as shown in Fig. 7b. With increasing the number of cycles, the UVC PSPL intensity decreases because the deep traps were gradually emptied.

### 3.7 Solar-blind optical tagging of $\text{Lu}_2\text{SiO}_5:\text{Pr}^{3+}$ phosphor

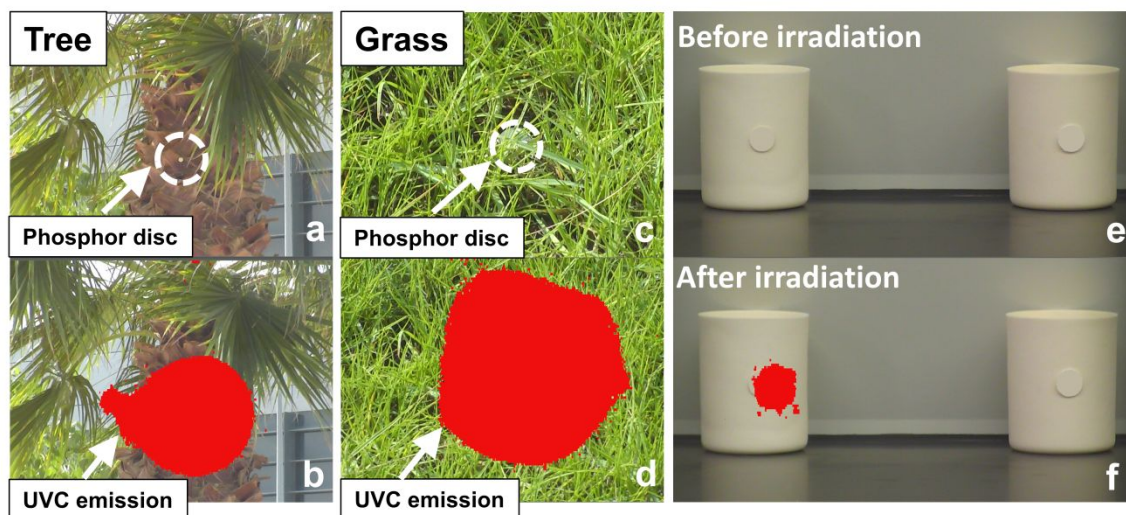


**Fig. 8** Solar-blind optical tagging application of  $\text{Lu}_2\text{SiO}_5:\text{Pr}^{3+}$  phosphor discs in various environmental conditions. The positions of the phosphor discs placed on the tree trunk (a) and in the grass (c) are indicated by dash-line circles, respectively. (b, d) The corresponding UVC imaging of the phosphor discs with the help of OFIL corona camera in direct sunlight. The samples were pre-irradiated by a 254 nm lamp for 2 min and the images were taken at about 5 min after ceasing the 254 nm UV lamp. The detected UVC emission is denoted by red pattern, whose area is proportional to the emission intensity. (e, f) An example application that makes use of the persistent UVC emission signal to differentiate two same cups. The two cups are labelled by  $\text{Lu}_2\text{SiO}_5:\text{Pr}^{3+}$  phosphor disc and ceramic disc (the same size but without UVC persistent luminescence), respectively.

In consideration of the long-lasting UVC persistent luminescence from  $\text{Lu}_2\text{SiO}_5:\text{Pr}^{3+}$  phosphor and zero UVC background on the Earth surface, the  $\text{Lu}_2\text{SiO}_5:\text{Pr}^{3+}$  phosphor can serve as remarkable identification tags to track and identify targets of interest in bright environments. To demonstrate the capability of  $\text{Lu}_2\text{SiO}_5:\text{Pr}^{3+}$  phosphor as covert optical taggants, UVC imaging experiments were carried out on the tree trunk and in the grass in

direct sunlight, as shown in Fig. 8a-d. Intense UVC afterglow emission from  $\text{Lu}_2\text{SiO}_5:\text{Pr}^{3+}$  phosphor can be clearly detected and imaged by the corona camera in bright outdoor environments after the stoppage of 254 nm UV excitation. To further confirm the optical tagging function, another tagging experiment was carried out to differentiate two same cups by using the persistent UVC emission signal. The two cups were labelled by  $\text{Lu}_2\text{SiO}_5:\text{Pr}^{3+}$  phosphor disc and ceramic disc (the same size but without UVC persistent luminescence). After irradiation by 254 nm UV lamp, the two cups can be clearly differentiated with the help of the UVC signal generated by the  $\text{Lu}_2\text{SiO}_5:\text{Pr}^{3+}$  phosphor, as shown in Fig. 8e and f. The capability to work in bright environments is the greatest advantage for UVC persistent phosphors when compared with visible and infrared phosphors because of the absence of interference from ambient lights. Besides, after irradiation by 254 nm UV light for 10 min, long-lasting UVC persistent emission can be clearly observed in an indoor-lighting environment (Supplementary Fig. S11). The UVC persistent emission signal gradually decreases as the decay time goes on, and the UVC signal is barely detected after 6 h decay. In addition to the indoor-lighting condition, the self-sustained UVC luminescence was also demonstrated in direct sunlight, as shown in Supplementary Fig. S12. It is found that direct sunlight illumination significantly reduces the afterglow time, and the UVC persistent luminescence signal in direct sunlight can only be monitored for 1 h. The decrease of UVC afterglow time in bright environments is the results of the dual effects of ambient heat stimulation (normal persistent luminescence) and photostimulation by ambient light (PSL).

#### **4. Conclusions**

In summary,  $\text{Lu}_2\text{SiO}_5:\text{Pr}^{3+}$  persistent phosphors have been synthesized via a sol-gel method followed by sintering at high temperature. The  $\text{Lu}_2\text{SiO}_5:\text{Pr}^{3+}$  phosphors can be charged effectively by a 254 nm mercury lamp and exhibits strong UVC persistent luminescence peaking at 270 nm and a long persistence time of more than 12 h. Moreover, enhanced UVC persistent luminescence can be repeatedly rejuvenated in pre-irradiated  $\text{Lu}_2\text{SiO}_5:\text{Pr}^{3+}$  sample after short-time low-energy white light illumination. The distinct spectral features of UVC light together with the self-sustained UVC luminescence property enable this material to act as covert optical taggants in bright indoor and outdoor environments. This  $\text{Lu}_2\text{SiO}_5:\text{Pr}^{3+}$  persistent phosphor is expected to find exciting applications in many important areas including environmental research, medical therapy, and solar-blind optical tagging.

### **Conflicts of interest**

There are no conflicts to declare.

### **Acknowledgements**

Y.L. acknowledges the financial support from the National Natural Science Foundation of China (grant no. 51902184), Shandong Provincial Natural Science Foundation (grant no. ZR2019BEM028) and the “Qi-Lu Young Scholar Fund” (grant no. 31370088963167) from Shandong University. Z.P. thanks the financial support from the US National Science Foundation (DMR-1705707) and the College of Petroleum Engineering and Geosciences, King Fahd University of Petroleum & Minerals.

### **References**

1. G. Matafonova and V. Batoev, *Water Res.*, 2018, **132**, 177.
2. E. L. Cates, M. Cho and J. H. Kim, *Environ. Sci. Technol.*, 2011, **45**, 3680.

3. S. Nayak, S. E. O'Donnell, C. M. Sales and R. V. Tikekar, *J. Agr. Food Chem.*, 2016, **64**, 4214.
4. X. He, E. Xie, M. S. Islim, A. A. Purwita, J. J. D. Mckendry, E. Gu, H. Haas and M. D. Dawson, *Photonics Res.*, 2019, **7**, B41.
5. O. Alkhazragi, F. C. Hu, P. Zou, Y. A. Ha, C. H. Kang, Y. Mao, T. K. Ng, N. Chi and B. S. Ooi, *Opt. Express*, 2020, **28**, 9111.
6. X. Chen, F. Ren, S. Gu and J. Ye, *Photonics Res.*, 2019, **7**, 381.
7. M. Buonanno, D. Welch, I. Shuryak and D. J. Brenner, *Sci. Rep.*, 2020, **10**, 10285.
8. L. Chen, L. Lin, M. Tian, X. Bian, L. Wang and Z. Guan, *Energy Power Eng.*, 2013, **5**, 1298.
9. J. Xu and S. Tanabe, *J. Lumin.*, 2019, **205**, 581.
10. Y. Liang, F. Liu, Y. Chen, K. Sun and Z. Pan, *Dalton Trans.*, 2016, **45**, 1322.
11. Y. Zhang, D. Chen, W. Wang, S. Yan, J. Liu and Y. Liang, *Inorg. Chem. Front.*, 2020, **7**, 3063.
12. K. Van den Eeckhout, P. F. Smet and D. Poelman, *Materials*, 2010, **3**, 2536.
13. H. F. Brito, J. Holsa, T. Laamanen, M. Lastusaari, M. Malkamaki and L. C. V. Rodrigues, *Opt. Mater. Express*, 2012, **2**, 371.
14. K. Van den Eeckhout, D. Poelman and P. F. Smet, *Materials*, 2013, **6**, 2789.
15. Y. Zhuang, Y. Katayama, J. Ueda and S. Tanabe, *Opt. Mater.*, 2014, **36**, 1907.
16. J. Xu, J. Ueda and S. Tanabe, *J. Am. Ceram. Soc.*, 2017, **100**, 4033.
17. Z. Zhou, Y. Li and M. Peng, *Chem. Eng. J.*, 2020, **399**, 125688.
18. H. Yamamoto and T. Matsuzawa, *J. Lumin.*, 1997, **72-74**, 287.

19. T. Matsuzawa, Y. Aoki, N. Takeuchi and Y. Murayama, *J. Electrochem. Soc.*, 1996, **143**, 2670.
20. J. Ueda, S. Miyano and S. Tanabe, *ACS Appl. Mater. Interfaces*, 2018, **10**, 20652.
21. Z. Wang, Z. Song, L. Ning and Q. Liu, *J. Mater. Chem. C*, 2020, **8**, 1143.
22. Z. Wang, Z. Song and Q. Liu, *Mater. Chem. Front.*, 2021, **5**, 333.
23. X. Wang, Z. Zhang, Z. Tang and Y. Lin, *Mater. Chem. Phys.*, 2003, **80**, 1.
24. Z. Pan, Y. Y. Lu and F. Liu, *Nat. Mater.*, 2012, **11**, 58.
25. Y. J. Liang, F. Liu, Y. F. Chen, X. J. Wang, K. N. Sun and Z. Pan, *Light Sci. Appl.*, 2016, **5**, e16124.
26. Y. Li, M. Gecevicius and J. Qiu, *Chem. Soc. Rev.*, 2016, **45**, 2090.
27. S. K. Sun, H. F. Wang and X. P. Yan, *Acc. Chem. Res.*, 2018, **51**, 1131.
28. J. Xu, D. Murata, J. Ueda, B. Viana and S. Tanabe, *Inorg. Chem.*, 2018, **57**, 5194.
29. Y. Zhuang, L. Wang, Y. Lv, T. L. Zhou and R. J. Xie, *Adv. Funct. Mater.*, 2018, **28**, 1705769.
30. F. Liu and X. J. Wang, *Chinese J. Lumin.*, 2017, **38**, 1.
31. A. M. Srivastava, *J. Lumin.*, 2016, **169**, 445.
32. J. T. W. Dehair, *J. Solid State Chem.*, 1980, **33**, 33.
33. A. M. Srivastava, M. T. Sobieraj, S. K. Ruan and E. Banks, *Mater. Res. Bull.*, 1986, **21**, 1455.
34. M. Broxtermann, D. den Engelsen, G. R. Fern, P. Harris, T. G. Ireland, T. Justel and J. Silver, *Ecs J. Solid State Sc.*, 2017, **6**, R47.
35. A. M. Srivastava, M. Jennings and J. Collins, *Opt. Mater.*, 2012, **34**, 1347.

36. Y. M. Yang, Z. Y. Li, J. Y. Zhang, Y. Lu, S. Q. Guo, Q. Zhao, X. Wang, Z. J. Yong, H. Li, J. P. Ma, Y. Kuroiwa, C. Moriyoshi, L. L. Hu, L. Y. Zhang, L. R. Zheng and H. T. Sun, *Light Sci. Appl.*, 2018, **7**, 88.
37. X. Wang, Y. Chen, F. Liu and Z. Pan, *Nat. Commun.*, 2020, **11**, 2040.
38. L. Pidol, O. Guillot-Noel, A. Kahn-Harari, B. Viana, D. Pelenc and D. Gourier, *J. Phys. Chem. Solids*, 2006, **67**, 643.
39. M. Nikl, H. Ogino, A. Yoshikawa, E. Mihokova, J. Pejchal, A. Beitlerova, A. Novoselov and T. Fukuda, *Chem. Phys. Lett.*, 2005, **410**, 218.
40. X. Zhang, J. Xie, X. Chen, L. Fan, D. Lin, Y. Wang and Y. Shi, *J. Alloy Compd.*, 2016, **656**, 735.
41. J. Ueda, P. Dorenbos, A. J. J. Bos, A. Meijerink and S. Tanabe, *J. Phys. Chem. C*, 2015, **119**, 25003.
42. J. Trojan-Piegza, J. Niittykoski, J. Holsa and E. Zych, *Chem. Mater.*, 2008, **20**, 2252.
43. C. J. Delbecq, Y. Toyozawa and P. H. Yuster, *Phys. Rev. B*, 1974, **9**, 4497.
44. F. Liu, W. Yan, Y. J. Chuang, Z. Zhen, J. Xie and Z. Pan, *Sci. Rep.*, 2013, **3**, 1554.
45. K. Van den Eeckhout, A. J. J. Bos, D. Poelman and P. F. Smet, *Phys. Rev. B*, 2013, **87**, 045126.
46. J. J. Joos, K. Korthout, L. Amidani, P. Glatzel, D. Poelman and P. F. Smet, *Phys. Rev. Lett.*, 2020, **125**, 033001.
47. A. J. J. Bos, R. M. van Duijvenvoorde, E. van der Kolk, W. Drozdowski and P. Dorenbos, *J. Lumin.*, 2011, **131**, 1465.
48. H. Sun, Q. Gao, A. Wang, Y. Liu, X. J. Wang and F. Liu, *Opt. Mater. Express*, 2020, **10**, 1296.

49. D. Van der Heggen, D. Vandenberghe, N. K. Moayed, J. De Grave, P. F. Smet and J. J. Joos, *J. Lumin.*, 2020, **226**,117496.